Trans-dimerization of JAM-A regulates Rap2 and is mediated by a domain that is distinct from the cis-dimerization interface

Ana C. Monteiro, *Emory University*
Anny-Claude Luissint, *Emory University*
Ronen Sumagin, *Emory University*
Caroline Lai, *Vanderbilt University School of Medicine*
Franziska Vielmuth, *Ludwig-Maximilians University*
Mattie F. Wolf, *Emory University*
Oskar Laur, *Emory University*
Kerstin Reiss, *University of Tübingen*
Volker Spindler, *Ludwig-Maximilians University*
Thilo Stehle, *Vanderbilt University School of Medicine*

Only first 10 authors above; see publication for full author list.

Journal Title: Molecular Biology of the Cell
Volume: Volume 25, Number 10
Publisher: American Society for Cell Biology | 2014-05-15, Pages 1574-1585
Type of Work: Article | Final Publisher PDF
Publisher DOI: 10.1091/mbc.E14-01-0018
Permanent URL: http://pid.emory.edu/ark:/25593/gk33c

Final published version: http://www.molbiolcell.org/content/25/10/1574

Copyright information:

Trans-dimerization of JAM-A regulates Rap2 and is mediated by a domain that is distinct from the *cis*-dimerization interface

Ana C. Monteiro[a], Anny-Claude Luissint[a], Ronen Sumagin[a], Caroline Lai[b,c], Franziska Vielmuth[d], Mattie F. Wolf[a], Oskar Laur[a], Kerstin Reiss[e], Volker Spindler[d], Thilo Stehle[c,e], Terence S. Dermody[b,c,f], Asma Nusrat[a], and Charles A. Parkos[a]

[a]Epithelial Pathobiology and Mucosal Inflammation Research Unit, Department of Pathology and Laboratory Medicine, Emory University School of Medicine, Atlanta, GA 30322; [b]Department of Pathology, Microbiology, and Immunology, [c]Elizabeth B. Lamb Center for Pediatric Research, and [f]Department of Pediatrics, Vanderbilt University School of Medicine, Nashville, TN 37232; [d]Institute of Anatomy and Cell Biology, Ludwig-Maximilians University, 80336 Munich, Germany; [e]Interfaculty Institute of Biochemistry, University of Tübingen, D-72076 Tübingen, Germany

ABSTRACT **Junctional adhesion molecule-A (JAM-A) is a tight junction–associated signaling protein that regulates epithelial cell proliferation, migration, and barrier function. JAM-A dimerization on a common cell surface (in *cis*) has been shown to regulate cell migration, and evidence suggests that JAM-A may form homodimers between cells (in *trans*). Indeed, transfection experiments revealed accumulation of JAM-A at sites between transfected cells, which was lost in cells expressing *cis*- or predicted *trans*-dimerization null mutants. Of importance, microspheres coated with JAM-A containing alanine substitutions to residues 43NNP45 (NNP-JAM-A) within the predicted *trans*-dimerization site did not aggregate. In contrast, beads coated with *cis*-null JAM-A demonstrated enhanced clustering similar to that observed with wild-type (WT) JAM-A. In addition, atomic force microscopy revealed decreased association forces in NNP-JAM-A compared with WT and *cis*-null JAM-A. Assessment of effects of JAM-A dimerization on cell signaling revealed that expression of *trans*- but not *cis*-null JAM-A mutants decreased Rap2 activity. Furthermore, confluent cells, which enable *trans*-dimerization, had enhanced Rap2 activity. Taken together, these results suggest that *trans*-dimerization of JAM-A occurs at a unique site and with different affinity compared with dimerization in *cis*. *Trans*-dimerization of JAM-A may thus act as a barrier-inducing molecular switch that is activated when cells become confluent.**

Monitoring Editor
Keith E. Mostov
University of California, San Francisco

Received: Jan 13, 2014
Revised: Mar 14, 2014
Accepted: Mar 14, 2014

INTRODUCTION

Junctional adhesion molecule-A (JAM-A) is a member of the immunoglobulin superfamily of proteins (IgSF) that localize to tight junctions (TJs) of polarized cells to regulate cell proliferation, cell migration, and barrier function (Mandell *et al.*, 2005; Naik *et al.*, 2008; Azari *et al.*, 2010; Nava *et al.*, 2011; Iden *et al.*, 2012; Monteiro *et al.*, 2013). As a single-span transmembrane protein, JAM-A initiates cytoplasmic signaling by associating with scaffolding proteins through its C-terminal PDZ-binding motif (Bazzoni *et al.*, 2000; Ebnet *et al.*, 2000; Mandell *et al.*, 2005; Severson *et al.*, 2008; Monteiro *et al.*, 2013). The N-terminal extracellular segment of JAM-A is composed of two extracellular Ig-like domains, the most distal of which (D1) mediates dimerization of JAM-A in *cis* (on the same cell surface), as confirmed by structural and biochemical studies (Prota, 2003). Crystallographic studies suggest that JAM-A also may form dimers in a *trans* conformation (across cells) at a site distinct from the motif involved in *cis*-dimerization (Kostrewa *et al.*, 2001; Prota, 2003). JAM-A *trans*-dimerization also has been

This article was published online ahead of print in MBoC in Press (http://www.molbiolcell.org/cgi/doi/10.1091/mbc.E14-01-0018) on March 26, 2014.

The authors declare no conflicts of interest.

Address correspondence to: Charles Parkos (cparkos@emory.edu).

Abbreviations used: PDZ-binding motif, postsynaptic density protein (PSD95), Drosophila disc large tumor suppressor (DlgA), and zonula occludens-1 protein (ZO-1)-binding motif; PDZ-GEF, PDZ domain containing guanine nucleotide exchange factor (GEF); Rap1, Ras-related protein 1; ZO, zonula occludens.

Supplemental Material can be found at:
http://www.molbiolcell.org/content/suppl/2014/03/24/mbc.E14-01-0018v1.DC1.html

supported by reports of JAM-A–dependent adhesion between platelets and endothelial cells (Babinska *et al.*, 2002a) and the observation that cells overexpressing JAM-A show accumulation of the protein at contacts between transfected cells (Ebnet *et al.*, 2000; Mandell *et al.*, 2004). However, the molecular basis and functional consequences of *trans* interactions between JAM-A molecules are not known.

Although definitive molecular evidence for JAM-A *trans*-homodimerization is lacking, there is structural evidence documenting dimerization in *cis* that mediates JAM-A function. Mutagenesis studies identified charged amino acids arginine 61 and glutamate 63 in the distalmost Ig-like domain that interact to form a salt bridge mediating *cis* interactions between two JAM-A molecules (Mandell *et al.*, 2004; Guglielmi *et al.*, 2007). Experiments using JAM-A mutants in which arginine 61 and glutamate 63 are exchanged with alanine (termed 6163) or the entire distal Ig-like domain is deleted (termed DL1) demonstrated important functional roles for *cis*-dimerization in epithelial cells. It was determined that JAM-A regulates cell migration and does so through association with the Rap exchange factor PDZ-GEF2 and the scaffold protein afadin to activate the small GTPase, Rap1, and subsequently stabilize β1 integrin on the cell surface (Severson *et al.*, 2009). However, overexpression of *cis*-null JAM-A mutant 6163 or DL1 in cells led to decreased β1 integrin expression and inhibition of cell migration (Severson *et al.*, 2008). Finally, cells expressing a JAM-A dimerization-null mutant lacking the distalmost Ig-like domain (DL1) exhibited enhanced proliferation compared with cells overexpressing WT JAM-A (Nava *et al.*, 2011).

Whereas previous studies focused on the functional importance of JAM-A *cis*-dimerization, the observation that exogenous JAM-A accumulates at cell contacts (Ebnet *et al.*, 2000; Mandell *et al.*, 2004) suggests that *trans*-dimerization may also be functionally important. We reasoned that simultaneous *cis*- and *trans*-dimerization of JAM-A could facilitate formation of oligomers that mediate signal transduction through clustering of associated proteins. Indeed, epithelial permeability and cell migration studies suggest that JAM-A dimerization is required to assemble groups of signaling proteins at the apical junctional complex (Bazzoni *et al.*, 2000; Severson *et al.*, 2009; Monteiro *et al.*, 2013). For example, JAM-A–mediated regulation of epithelial permeability was shown to depend on JAM-A interactions with ZO proteins, afadin, and PDZ-GEF1, which activate Rap2c and regulate the dynamics of the apically associated actomysosin belt (Monteiro *et al.*, 2013). However, despite the clear link between JAM-A and regulation of epithelial permeability, the role of dimerization has not been defined.

In this study, we determine whether JAM-A mutants incapable of forming *trans*- and/or *cis*-dimers differentially regulate JAM-A effectors implicated in epithelial function. We find that JAM-A *trans*-dimerization occurs both in cells and between surfaces coated with recombinant JAM-A. Furthermore, we identify putative motifs for *trans*-dimerization and suggest a functional role for JAM-A *trans*-dimer formation in epithelial cell signaling.

RESULTS

Recombinant soluble JAM-A forms homodimers in a pH-dependent manner

To investigate properties of JAM-A homodimerization, we analyzed recombinant soluble JAM-A ectodomains consisting of the two extracellular Ig-like domains by size-exclusion chromatography to determine the Stokes radius. Dimerization was assessed using several different buffer conditions, with pH values ranging from 5 to 8. Size-exclusion chromatography of soluble, full-length segments of extracellular JAM-A resuspended in calcium-free, Tris-based buffers at pH 8 revealed a prominent elution peak at 41 kDa (Figure 1A). Given that soluble JAM-A monomers have a predicted molecular weight of 25 kDa and dimers have a predicted molecular weight of 50 kDa based on SDS–PAGE analysis, the peak observed using size-exclusion chromatography suggests that under native conditions JAM-A is a dimer, as previously reported (Guglielmi *et al.*, 2007).

To confirm the Stokes radius of monomeric JAM-A by size-exclusion chromatography, we analyzed elution peaks for soluble, extracellular segments of a JAM-A mutant lacking the *cis*-dimerization motif (6163 JAM-A). Size-exclusion chromatography of soluble extracellular segments of 6163 JAM-A in Tris buffer at pH 8 revealed a single peak with a Stokes radius that corresponds to an apparent molecular weight of 29 kDa (Figure 1B). Together these results suggest that monomeric JAM-A has a Stokes radius corresponding to ~29 kDa at pH 8 and that soluble, extracellular segments of JAM-A preferentially form dimers under native conditions.

Although soluble JAM-A ectodomains form dimers at pH 8, size-exclusion chromatography experiments using JAM-A ectodomains performed in pH 5 citrate buffer revealed a single elution peak equivalent to 25 kDa (Figure 1C), consistent with JAM-A monomers.

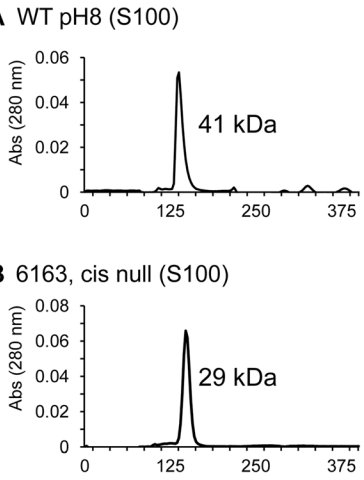

C

	Elution Volume (ml)	Stokes Radius (kDa)	Status
WT pH8 (S100)	136.3	40.6	Dimer
6163_JAM-A (S100)	147.5	29.3	Monomer
WT pH6.9 (S100)	128.5	49.4	Dimer
WT pH5.6 (S300)	233.6	28.1	Monomer
WT pH5 (S300)	238.4	24.3	Monomer
WT ph5 to 8 (S300)	218.9	43.7	Dimer
WT pH5.6 to 8 (S300)	218.9	43.7	Dimer
DL1_JAM-A (S100)	173.7	17.7	Monomer

FIGURE 1: JAM-A forms homodimers in a pH-dependent manner. (A) Size-exclusion chromatography of JAM-A was performed in Tris-buffered saline at pH 8. (B) *cis*-Dimerization–null JAM-A mutant (6163 JAM-A) was assessed by size-exclusion chromatography. Size-exclusion chromatography values for JAM-A and mutants eluted at different buffer conditions and column size (S100 or S300 as indicated). (C) Elution volume, calculated Stokes radius, and dimerization status.

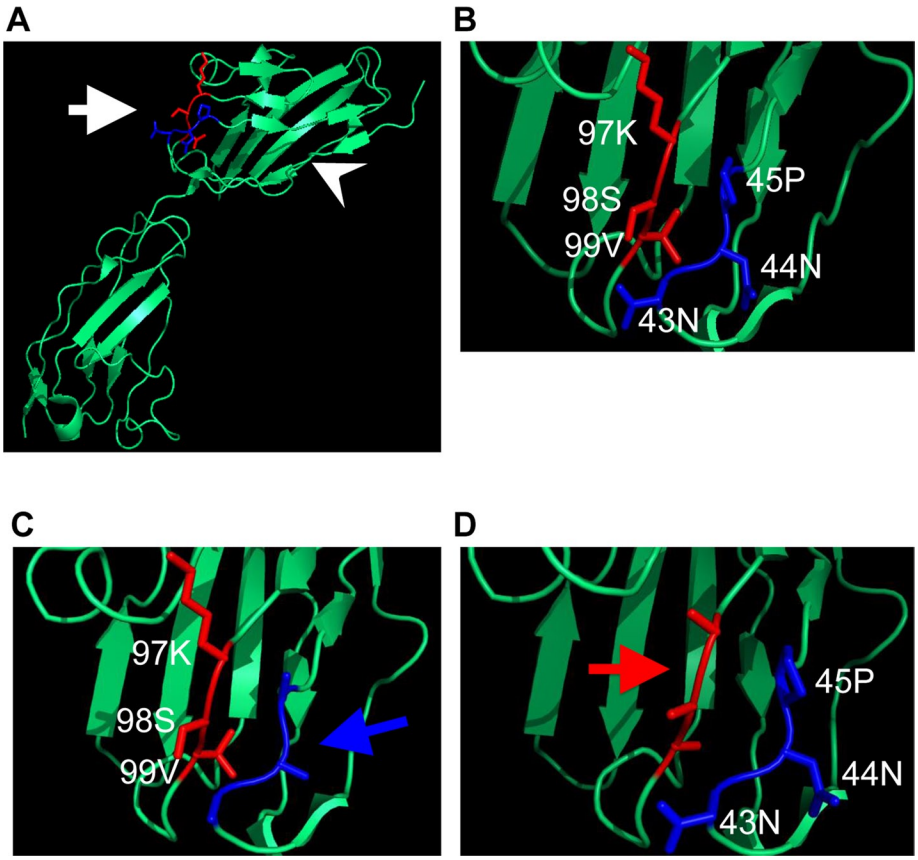

FIGURE 2: JAM-A mutants have alterations in the putative *trans*-dimerization interface. (A) JAM-A *cis*-dimerization occurs by ionic interactions between residues located on the C, C′, F, G β-sheet of the D1 domain (arrowhead), whereas *trans*-dimerization is predicted to occur on the opposite face of D1 (arrow). (B) The predicted site for *trans*-dimerization involves two motifs composed of residues N43–P45 and K97–V99, which combine to form a groove. The NNP mutant contains alanine substitutions of amino acids N43–P45 (C, blue arrow), and the KSV mutant contains alanine substitutions of amino acids K97–V99 (D, red arrow).

Elution of JAM-A at pH 5.6 revealed a major peak equivalent to 28 kDa (Figure 1C), also consistent with monomeric JAM-A. Size-exclusion chromatography of WT JAM-A incubated in pH 6.9 buffer revealed a single peak equivalent to 50 kDa, suggesting that disruption of JAM-A dimers occurs between pH 5 and 6.9 (Figure 1C), consistent with previous reports that murine JAM-A dimers dissociate in acidic conditions (Bazzoni *et al.*, 2000). To ensure that disruption of JAM-A dimers at low pH was not due to protein denaturation, we performed size-exclusion chromatography of soluble extracellular JAM-A that was first incubated at pH 5 or 5.6, followed by adjustment to pH 8. Elution fractions corresponding to monomeric JAM-A that had been resuspended at pH 5 or 5.6 and adjusted to pH 8 before size-exclusion chromatography revealed a peak of the Stokes radius equivalent to 45 kDa (Figure 1C), consistent with a dimeric form of JAM-A. These observations suggest that pH-dependent disruption of JAM-A dimerization is reversible. It is thus possible that the pH dependence of dimerization may play a role in intracellular trafficking of JAM-A, in which low endosomal/lysosomal pH could potentially inhibit dimerization-dependent signaling events.

Identification of JAM-A *trans*-dimerization sites by site-directed mutagenesis

The chromatography studies in Figure 1, A–C, indicate that JAM-A ectodomains form pH-sensitive homodimers, which is consistent with previous studies that explored a functional role for JAM-A *cis*-dimerization (Bazzoni *et al.*, 2000; Severson *et al.*, 2008). However, crystallographic analyses (Kostrewa *et al.*, 2001) raise the possibility that JAM-A forms *trans*-dimers using sequences distinct from those required for *cis*-dimerization. These studies identified a potential site for *trans*-dimerization on the protein surface opposite to that used for *cis*-dimerization on the distal Ig-like domain of JAM-A.

Because the size-exclusion chromatography studies did not reveal JAM-A complexes larger than dimers, we considered the possibility that *trans*-dimers interact with low affinity. To investigate whether JAM-A forms homodimers across cells (in *trans*) and identify sites of JAM-A *trans*-dimerization, we performed mutagenesis of full-length JAM-A, followed by transfection and determination of distribution between expressing cells. Two new constructs were designed containing alanine substitutions within a putative *trans*-dimerization region located in the D1 domain on the surface opposite to the *cis*-dimerization motif (Figure 2A), as predicted from the crystal structure of murine JAM-A and platelet adhesion studies (Kostrewa *et al.*, 2001; Babinska *et al.*, 2002b). The two putative *trans*-dimerization–null mutants have alterations that correspond to distinct motifs on the D1 domain, which combine to form a three-dimensional groove that might be a favorable site for *trans*-dimerization mediated by nonionic interaction forces (Figure 2B). The NNP mutant protein has alanine substitutions of glutamine 43, glutamine 44, and proline 45 in the predicted *trans*-dimerization motif (Figure 2C). The KSV mutant protein has alanine substitutions of lysine 97, serine 98, and valine 99 (Figure 2D).

JAM-A *trans*-dimerization was assessed by overexpressing full-length WT JAM-A (Figure 3A) and the mutant JAM-A constructs (Figure 3, B–E) in CHO cells, which have no detectable endogenous JAM-A. Using immunofluorescence, we evaluated whether the JAM-A mutant proteins accumulated at intercellular contacts. Surface expression of each mutant was confirmed by flow cytometry. Three independent transient transfections of CHO cells with plasmids encoding WT or mutant JAM-A led to similar levels of JAM-A surface expression as assessed by flow cytometry (Supplemental Figure S1). For confocal microscopy, transfected CHO cells were costained with a rabbit polyclonal antibody (pAb) against the JAM-A cytoplasmic tail and a murine monoclonal antibody (mAb) against a conformational epitope surrounding residue N117 in the D1 domain (J10.4; Mandell *et al.*, 2004; Severson *et al.*, 2009). Predictably, all JAM-A mutant proteins were detectable using the mAb J10.4, with the exception of DLI JAM-A, which lacks D1 and as such was only detectable with the pAb against the JAM-A cytoplasmic tail. Consistent with previous observations (Ebnet *et al.*, 2001; Mandell *et al.*, 2004), we found that exogenous WT JAM-A accumulated at contacts between JAM-A–expressing CHO cells (Figure 3F, highlighted with arrows). However, DL1 JAM-A, which lacks the D1

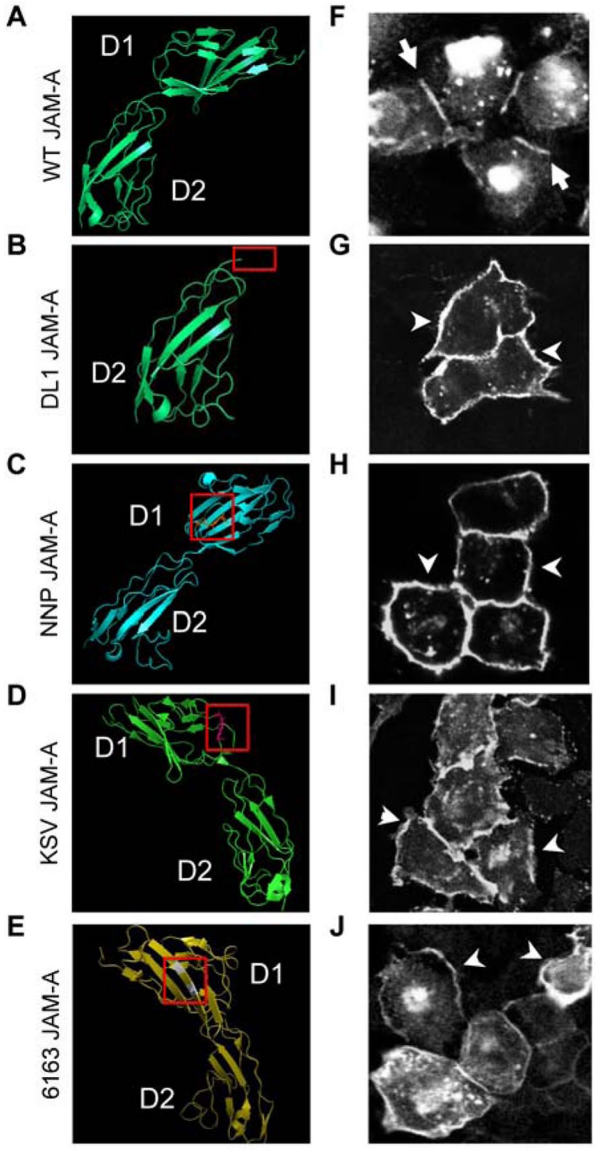

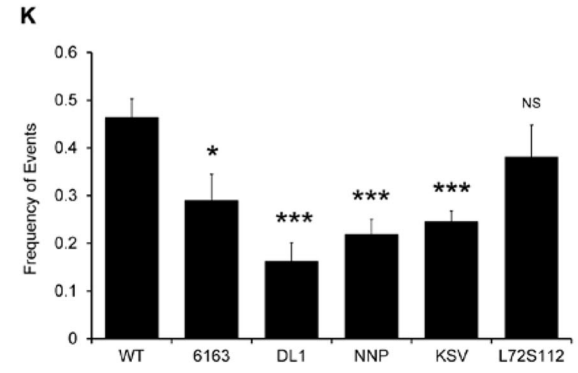

FIGURE 3: Subcellular localization of JAM-A mutants. (A–E) JAM-A *cis*- and predicted *trans*-dimer mutants were engineered using site-directed mutagenesis. (A) WT JAM-A is composed of two extracellular Ig-like domains, the most distal of which (D1) is involved in JAM-A homodimerization. (B) DL1 JAM-A lacks the entire membrane-distal Ig-like domain, with only the membrane proximal domain (D2) remaining. (C) NNP JAM-A has alanine substitutions of amino acids 43N, 44N, and 45P, which are predicted to be involved in *trans*-dimerization. (D) KSV JAM-A has alanine substitutions of amino acids 96K, 97S, and 99V, which compose the second motif predicted to be involved in *trans*-dimerization. (E) 6163 JAM-A has alanine substitutions of amino acids 61E and 63K, previously implicated in JAM-A *cis*-dimerization. (F–J) CHO cells were transfected with WT and mutant JAM-A and fixed for immunofluorescence staining and confocal microscopy after 48 h. Subcellular localization of exogenously expressed mutants elucidate sites on JAM-A required for *trans*-dimerization. WT JAM-A accumulated only at cell–cell contacts between JAM-A–expressing cells. All JAM-A mutants diffusely localized on the cell surface, even in areas of cell–cell contact between transfected and nontransfected cells (arrowheads). Distribution of WT and mutant JAM-A expressed in CHO cells was quantified as a ratio of cells with junction-localized JAM-A between JAM-A–positive cells to total number of JAM-A–positive cells per field. (K) A JAM-A isoform with functionally irrelevant cysteine substitutions at Leu-72 and Ser-112 (L72S112) distributed to junctions at a rate statistically similar to WT JAM-A ($n > 8$ fields, collected for >3 different transfections; mean ± SEM; ***$p < 0.001$; *$p < 0.05$; NS, $p > 0.2$).

domain, did not preferentially distribute to contacts between JAM-A–expressing cells but instead was dispersed diffusely at the cell periphery (Figure 3G, arrowheads). This pattern of distribution suggests that motifs located in the D1 domain are required for concentration of JAM-A between cells. Of interest, NNP and KSV JAM-A also distributed diffusedly on the surface of CHO cells and was not restricted to cell–cell contacts between transfected cells (Figure 3, H and I, arrowheads). Consistent with previous observations (Mandell *et al.*, 2004), the JAM-A mutant with alteration at residues 61 and 63 required for *cis*-dimerization (6163 JAM-A) also diffusely localized on the cell surface, even in areas of cell–cell contact between transfected and nontransfected cells (arrowheads; Figure 3J). Quantification of the frequency of JAM-A accumulation at cell–cell contacts, calculated as the percentage of cells expressing JAM-A predominantly at junctions between two transfected cells relative to the total number of cells expressing JAM-A, revealed that 46% (±4% SEM) of cells expressing WT JAM-A displayed localization of JAM-A to contacts between JAM-expressing cells. In contrast, analyses of cells expressing DL1, 6163, NNP, and KSV mutants revealed significantly reduced JAM-A distribution to cell contacts, with frequencies of 16 (±4 SEM), 30 (±5 SEM), 22 (±3 SEM), and 25% (±2% SEM), respectively (Figure 3K). To ascertain that the results in Figure 3 represented loss-of-function effects specific to the altered residues and that mutagenesis itself was not nonspecifically affecting the localization of JAM-A, we also quantified the rate of JAM-A distribution to contacts of cells expressing a JAM-A mutant protein containing cysteine substitutions at residues lysine 72 and serine 112 in the D1 domain. Of importance, this JAM-A mutant accumulated at junctions at a similar frequency as observed for WT JAM-A (Figure 3K and Supplemental Figure S2), indicating that not all mutations affect the accumulation of JAM-A at cell contacts. These findings indicate that the motifs altered by the 6163, NNP, and KSV mutations are important for the interaction of JAM-A across cells.

Although analysis of the subcellular localization of WT and mutant JAM-A in Figure 3 suggested that both *cis* and *trans* motifs are required for localization of JAM-A at cell–cell junctions, we performed additional experiments to test whether mutation of the *trans*-dimerization motifs globally alters the tertiary structure of JAM-A. Recognition by mAb J10.4, which binds a conformational epitope on the D1 domain of JAM-A (Mandell *et al.*, 2004), was retained in all JAM-A mutants with the exception of DLI JAM-A, suggesting that these mutations do not globally alter the tertiary

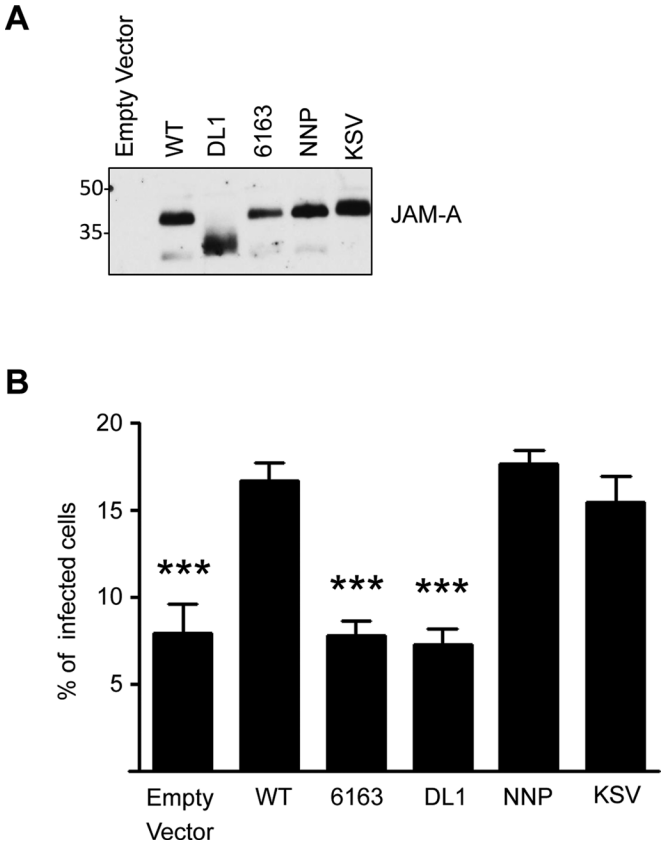

FIGURE 4: Alteration of JAM-A residues does not affect reovirus infectivity. CHO cells were transfected with the plasmids shown. JAM-A expression and reovirus infectivity in these cells were determined 48 h posttransfection. (A) For expression analysis, cells were harvested in RIPA buffer and stained with rabbit pAb against the cytoplasmic, C-terminal domain by immunoblotting. (B) For infectivity assessment, CHO cells were adsorbed with T3 reovirus at an MOI of 100 PFUs/cell at 37°C for 1 h, washed twice, and incubated at 37°C in fresh medium. After 20–24 h incubation, cells were harvested and stained with Alexa Fluor–conjugated reovirus-specific antiserum. The percentage of infected cells was quantified using flow cytometry ($n = 3$ independent experiments; mean ± SEM; ***$p < 0.001$ compared with WT).

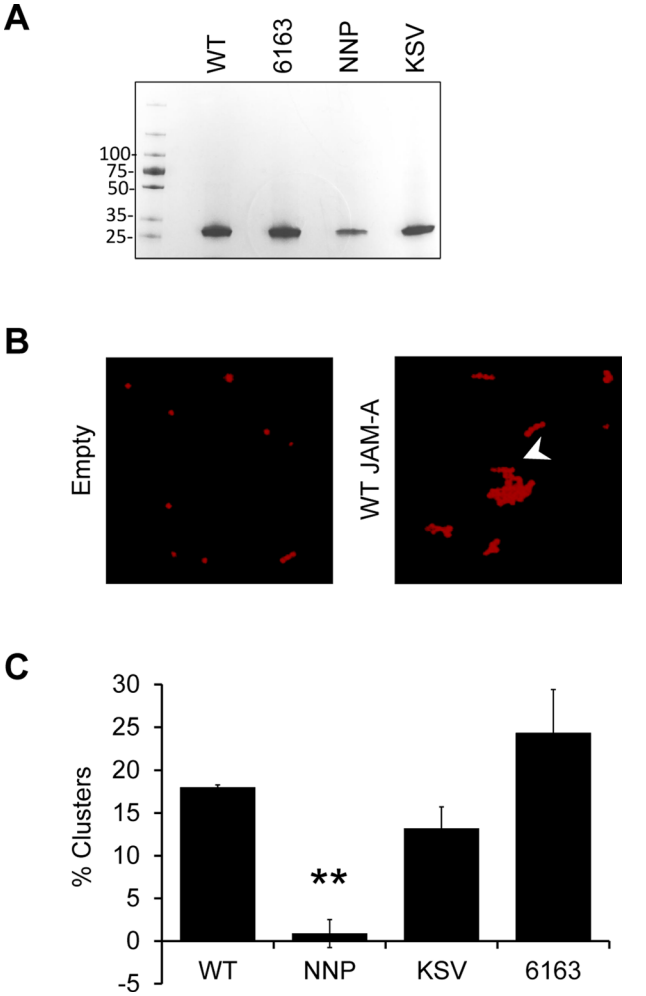

FIGURE 5: JAM-A–conjugated beads cluster as determined by flow cytometry. (A) Bacterially expressed recombinant ectodomains of WT and mutant JAM-A with a C-terminal His tag were purified and analyzed by SDS–PAGE. (B) His-binding 1-μm beads conjugated to His-tagged WT JAM-A clustered in solution (arrowhead) compared with unconjugated beads. Bead clustering was quantified by assessing side and forward scatter using flow cytometry, by which frequency of unclustered beads was measured as a function of total beads. Flow cytometry data were pooled, and the frequency of clustering was calculated by subtracting frequency of unclustered beads from 100%. Baseline clustering observed in unconjugated beads (frequency ~30%) was considered to be background and was subtracted from the final readings observed in experiments using WT, NNP, KSV, and 6163 JAM-A–conjugated beads (C; $n > 3$ per group, mean ± SEM. **$p < 0.01$ compared with WT).

structure of JAM-A. We further assessed the mutant proteins for functional effects on reovirus infection, which is dependent on binding to JAM-A (Guglielmi *et al.*, 2007; Antar *et al.*, 2009). The *cis*-dimerization interface of JAM-A mediates reovirus attachment and infection (Guglielmi *et al.*, 2007; Kirchner *et al.*, 2008). Having confirmed expression of the mutant JAM-A proteins by immunoblotting (Figure 4A) and flow cytometry (Supplemental Figure S1), we inoculated CHO cells expressing 6163 or DL1 JAM-A with reovirus and observed that infection rates were significantly lower than those observed in CHO cells expressing WT JAM-A (Figure 4B), which is consistent with previous reports (Forrest, 2003; Guglielmi *et al.*, 2007). Of importance, reovirus infection did not differ significantly between CHO cells expressing WT or the *trans*-null mutants KSV or NNP (Figure 4C). Taken together, these results suggest that alanine substitutions at the *trans*-dimerization interface do not globally alter the tertiary structure of JAM-A.

Immunofluorescence staining and confocal analysis of CHO cells expressing WT or mutant JAM-A suggested that *cis*- and *trans*-dimerization of JAM-A is required for maximal accumulation of JAM-A at cell–cell contacts. To determine whether JAM-A forms dimers independent of other cellular proteins, we used an in vitro bead-based clustering assay. Soluble, C-terminally histidine (His)-tagged extracellular domains of WT JAM-A and each of the JAM-A mutants were expressed in bacteria and purified (Figure 5A). Soluble extracellular domains of His-tagged WT or mutant JAM-A proteins were conjugated to 1-μm nickel-coated beads, allowing for controlled orientation of JAM-A with the distal D1 domain facing away from the beads. With use of these JAM-A–coated beads, *trans*-dimerization events would be expected to result in enhanced clustering compared with control uncoated beads, as is observed by immunofluorescence labeling and confocal imaging in Figure 5B. Clustering events were quantified by flow cytometric determination of forward and side

scatter. Flow cytometric analysis of uncoated beads revealed that 70% of beads were not clustered, suggesting that uncoated beads nonspecifically interact (cluster) 30% of the time. Of interest, beads conjugated with His-tagged WT JAM-A formed higher-order clusters at a significantly higher rate than beads alone (48 vs. 30%, $p < 0.001$, Figure 5C). His-tagged *cis*-dimer null mutant (6163) JAM-A–coated beads did not cluster differently than observed with beads coated with WT JAM-A (54 vs. 30% for beads alone, $p > 0.3$ when compared with WT), suggesting that the *cis*-dimerization motif is not required for *trans* interactions in vitro (Figure 5C). Of importance, beads conjugated with His-tagged NNP, a *trans*-null mutant, failed to cluster, with values similar to empty control beads (<1% above beads alone, $p > 0.7$, $p < 0.001$ when compared with WT), suggesting that the NNP residues are required for JAM-A–dependent bead clustering. Beads conjugated with the NNP mutant had lower rates of clustering than beads conjugated with the KSV mutant (<1 vs. >13%, $p > 0.05$). Clustering of beads loaded with the KSV mutant also was lower than that observed for beads loaded with WT JAM-A. However, this difference was not statistically different (13 vs. 18% of clustering above background). These observations indicate that although the NNP and KSV residues are important for *trans*-dimerization in the bead-clustering assay, it is likely that the NNP residues are more important for JAM-A *trans*-dimerization in vitro than the KSV residues. To ensure that clustering effects were not caused by differential loading of proteins onto beads, we used flow cytometry to confirm that the total protein content of beads conjugated with NNP, KSV, or WT JAM-A did not differ (Supplemental Figure S3). Because the 6163 mutation did not affect *trans*-dimerization in the bead-clustering assays (Figure 5) and *cis*-dimerization motif–dependent reovirus infection experiments in Figure 5 showed no effect of NNP and KSV mutations on reovirus entry, these findings strongly suggest that *trans*- and *cis*-dimerization are mediated by distinct motifs on JAM-A that act independently.

Atomic force microscopy defines dimerization properties of JAM-A

To define the biophysical profile of JAM-A homodimerization at the single-molecule level, we used atomic force microscopy (AFM). Soluble His-tagged extracellular domains of WT or mutant JAM-A proteins were bound to AFM tips and substrate using amide-linkage reactions. Amide linkage allowed for JAM-A immobilization in parallel and antiparallel conformations that enabled both *cis*- and *trans*-dimerization events. Binding-event frequency was assessed by considering the deflection of the cantilever during movement of the tip toward and away from the substrate. Binding-frequency analysis (Figure 6A) revealed that the *cis*-null mutant (6163 JAM-A) displayed significantly less frequent homodimerization events than WT JAM-A (4.2 vs. 13.3% for all force curves, respectively, $p < 0.001$). NNP JAM-A, which lacks the motif for *trans*-dimerization as determined by bead-clustering assays (Figure 5C), also showed lower binding frequencies than WT JAM-A (11.7 vs. 13.3%, respectively), although these differences were not statistically significant. Pretreatment of WT, 6163, or NNP JAM-A–coated surfaces with J10.4 Fab′ fragment significantly reduced the binding events. WT JAM-A binding was reduced from 13.3 to 3.1% ($p < 0.001$), 6163 binding was reduced from 4.2 to 3.2% ($p < 0.05$), and NNP binding was reduced from 11.7 to 2.1% ($p < 0.001$). These findings suggest that compared with *trans*-dimerization, JAM-A *cis*-dimerization occurs at higher detectable frequencies with AFM. In addition, these results suggest that J10.4 Fab′ fragments inhibit both *cis*- and *trans*-dimerization events, since binding detected between 6163 mutants (4.2%) was further reduced with addition of J10.4 Fab′.

Owing to the spring characteristics of the AFM cantilevers, unbinding forces were derived from application of Hooke's law. Force of binding between WT or mutant JAM-A homodimers was deduced by calculating the unbinding force required to disrupt JAM-A interactions observed at different cantilever retraction speeds ranging from 1 to 10 μm/s. Assessment of the average binding force observed for all binding events at a particular retraction speed revealed that WT JAM-A forms homodimers with greater force at higher retraction speeds, as observed for other junction-associated proteins (Baumgartner *et al.*, 2000; Vedula *et al.*, 2008; Spindler *et al.*, 2009; Zhang *et al.*, 2010). At a pulling speed of 5 μm/s, homodimerization of WT JAM-A ectodomains was on average 133 pN (Figure 6B). In comparison, at a speed of 5 μm/s, the force of interacting *cis*-null 6163 JAM-A was on average 140 pN. Finally, ectodomains of *trans*-null NNP JAM-A displayed an average interaction force of 116 pN at the same speed. The difference in unbinding force detected between WT, 6163, and NNP mutants was similar with different pulling speeds. However, force differences between 6163 and WT JAM-A were significant only at two speeds (1 and 5 μm/s, but not 2.5 and 10 μm/s), whereas binding forces between JAM-A NNP ectodomains were significantly lower than forces between WT JAM-A at all loading rates. These data suggest that compared with WT JAM-A, *trans*-null (NNP) JAM-A mutants interact with weaker forces ($p < 0.001$) at the single-molecule level.

Finally, by assessing the peak unbinding force at different loading rates in a range from 10^4 to 10^5 pN/s, we derived the unstressed off rates for homodimerization of WT and mutant JAM-A according to Bell's model (Bell, 1978; Baumgartner *et al.*, 2000). Of interest, the highest off rate was calculated for WT JAM-A (0.24 s^{-1}), followed by NNP (0.2 s^{-1}) and 6163 (0.14 s^{-1}). These calculations suggest that WT JAM-A dimers have slightly shorter bond half-life and 6163 JAM-A dimers have the longest.

Identification of JAM-A *trans*-dimerization–dependent cell signaling events

JAM-A interacts with a scaffold protein complex that signals to regulate epithelial permeability through activation of the small GTPase Rap2 (Monteiro *et al.*, 2013). However, it is not known whether this signaling module is dependent on dimerization of JAM-A. Given our results indicating that specific regions in the D1 domain of JAM-A mediate dimerization between cells in *trans*, we transiently transfected full-length WT and dimerization mutant JAM-A in HEK-293T cells and compared the effects of disrupting *cis*- and *trans*-dimerization on JAM-A regulation of signals that trigger barrier function. Because loss of JAM-A in epithelial cells results in enhanced permeability linked to decreased levels of active Rap2 (Monteiro *et al.*, 2013), we assessed whether Rap2 activity was altered by expression of WT or mutant JAM-A. HEK-293T cells overexpressing WT JAM-A demonstrated enhanced activity of Rap2 (Figure 7A), which corroborates previous observations of decreased Rap2 activity in JAM-A–deficient cell lines. HEK-293T cells expressing *trans*-dimerization–null mutants NNP and KSV JAM-A displayed lower Rap2 levels and activity than WT JAM-A transfected cells. Total Rap2 activity, assessed as the signal of active Rap2 standardized to a tubulin loading control, suggested that *trans*-dimerization is required for the activation of Rap2 (Figure 7A). In contrast, lysates of HEK-293T cells overexpressing 6163 JAM-A, which exclusively lacks the *cis*-dimerization motif, did not display reduced activity of Rap2 compared with HEK-293T cells expressing WT JAM-A. These results suggest that JAM-A *trans*- but not *cis*-dimerization enhances Rap2

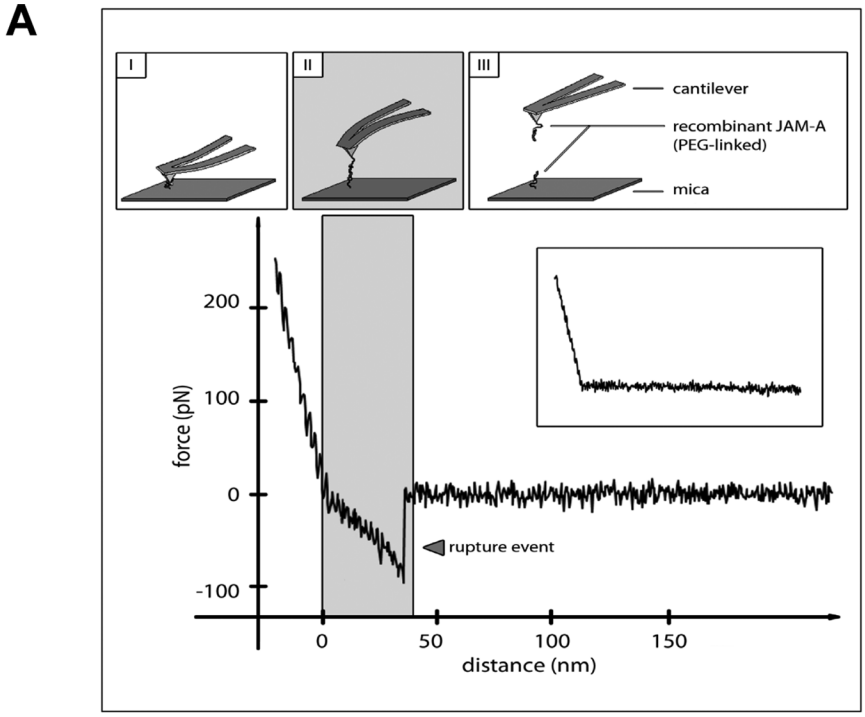

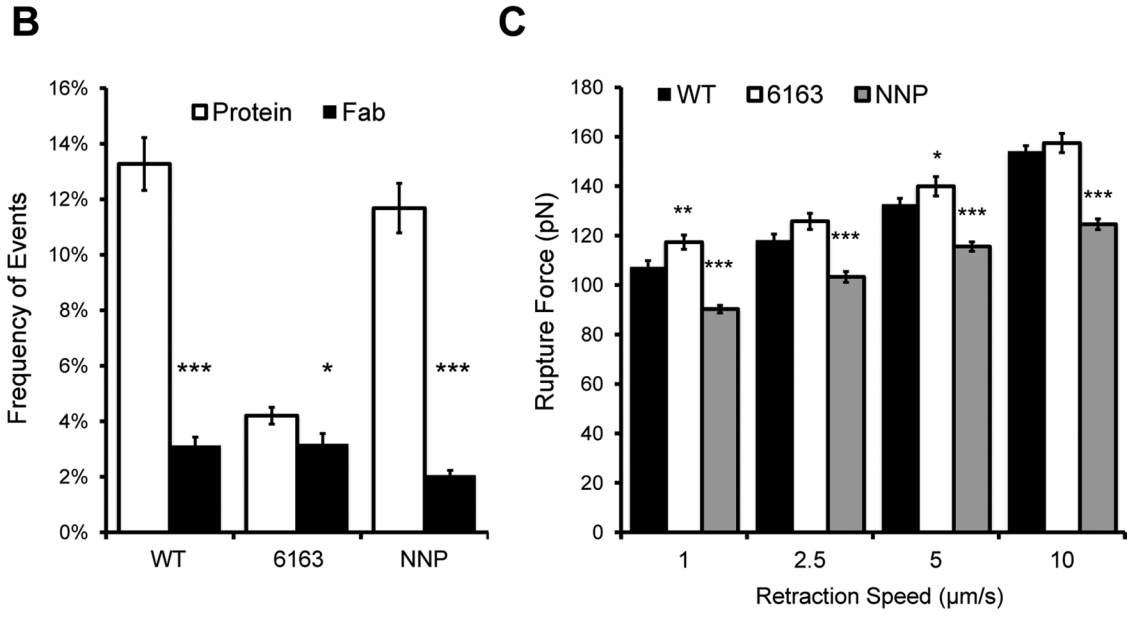

D

	K_{off} (s^{-1})
WT JAM-A	0.243
6163 JAM-A	0.138
NNP JAM-A	0.204

FIGURE 6: Atomic force microscopy reveals that JAM-A can form *cis*- and *trans*-dimers. (A) Principle of AFM force spectroscopy. A flexible cantilever (nominal spring constant 0.03 N/m), functionalized with recombinant JAM-A, is lowered onto a mica sheet also coated with the same JAM-A molecules until the cantilever is observed to be bending slightly upward (I). In the event of binding interactions between molecules on the cantilever and mica sheet, as the cantilever is retracted, it bends downward, and the forces are quantified. Forces acting on the cantilever are determined

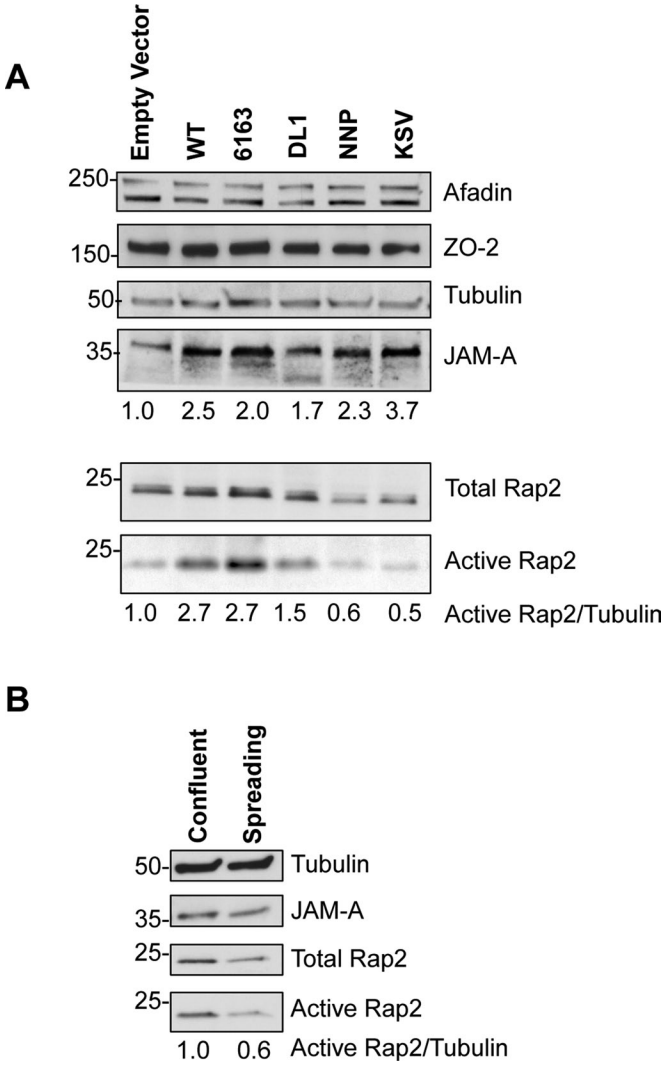

FIGURE 7: JAM-A *trans*- but not *cis*-dimerization is required for Rap2 activity. (A) WT and mutant JAM-A were expressed in HEK-293T cells. Cells were assessed for Rap2 activity by Ral-GDS precipitation. (B) Rap2 activity in confluent or spreading human intestinal epithelial cells (SK-CO15) was assessed with Ral-GDS precipitation.

activity in cells. Because JAM-A *trans*-dimerization events are, by definition, dependent on contacts between adjacent cells, we tested whether Rap2 activity was increased in confluent epithelial cell monolayers. As seen in Figure 7B, Rap2 activity was almost twofold higher in confluent monolayers of epithelial cells than in subconfluent cultures of spreading cells.

Collectively the findings presented suggest that *trans*-dimerization occurs at a site distinct from that mediating dimerization in *cis*, and, despite being a lower-affinity binding event, dimerization in *trans* mediates specific signaling events that regulate activation of Rap2. As illustrated in the model in Figure 8, we propose that JAM-A on the surface of subconfluent single cells does not activate barrier-inducing signals. However, JAM-A on confluent cells *trans*-dimerizes to form JAM-A multimers, which are required for inducing signals that regulate barrier function.

DISCUSSION

In this study, we demonstrate that JAM-A forms homodimers in *trans* at a site distinct from that used to form dimers in *cis*. *Trans*-dimerization of JAM-A occurs through lower-probability interactions mediated by the distal Ig-like domain at a site directly opposite to the *cis*-dimerization interface. Disruption of *trans*-dimerization by mutagenesis results in alterations in small GTPase signaling implicated in regulation of epithelial barrier function. On the basis of the observations presented in this article, we propose a model in which *trans*-dimerization–dependent JAM-A multimers initiate signaling events that are distinct from those initiated by *cis*-dimerization alone (Figure 8).

JAM-A *trans*-dimerization has been predicted by crystallographic studies of recombinant JAM-A ectodomains and in studies of JAM-A–dependent interactions between human platelets and endothelial cells. Before this study, there had been no investigations using biochemical and cell biological approaches to test whether JAM-A *trans*-dimerization occurs in nature and is functionally relevant.

By expressing WT and mutant forms of JAM-A in CHO cells, we observed that expression of either *cis*- or *trans*-dimerization–deficient mutants exhibited lower rates of JAM-A localization to cell–cell contacts, indicating a role for JAM-A oligomerization at cell junctions (Figure 3). We interpret these findings to suggest that JAM-A *cis*-dimerization is required to provide the necessary avidity for *trans*-dimerization to occur. In analogous studies, members of the cadherin family of proteins *trans*-dimerize and accumulate laterally at junctions to form zipper-like cadherin multimers (Brieher, 1996; Takeda *et al.*, 1999; Baumgartner *et al.*, 2000; Zhang *et al.*, 2010). Consistent with this idea, JAM-A *cis*-dimerization is predicted to occur at higher frequency than *trans*-dimerization, likely due to the charged residues involved in JAM-A *cis*-dimerization that establish a salt bridge between JAM-A monomers (Mandell *et al.*, 2004), whereas JAM-A *trans*-dimerization would occur by van der Waals forces between mostly uncharged polar residues. These predictions are supported by the chromatography results shown in Figure 1, which reveal the existence of *cis*-dimers but no higher-order multimers, which were disrupted by the *cis*-null (6163) mutation.

AFM analysis of purified JAM-A ectodomains detected both *cis*- and *trans*-dimerization events. However, *cis*-dimerization was detected more frequently, suggesting that it is a higher-probability interaction than *trans*-dimerization, likely due to ionic interactions between charged residues of the *cis*-dimerization motif. This supports a model in which higher-probability *cis*-dimerization events may supply the necessary avidity for JAM-A *trans*-dimerization and, as oligomers are formed, *trans*-dimerization events become more favorable and stabilize JAM-A oligomers. On the other hand, assessment of binding forces and off rates (Figure 6, B and C) suggested that when *trans*-dimerization occurs, as observed in binding events between *cis*-null

relative to distance from the mica sheet (II). When the force exerted by retracting the cantilever exceeds the force by which the JAM-A molecules interact, the bond ruptures and the cantilever returns to the baseline unbound state, indicated by the step in the force–distance graph. The cantilever is further retracted, and a new approach-retrace cycle can begin (III). Inset, an example force curve without any rupture event. AFM tip and substrate were coupled with WT, 6163 (*cis*-null), or NNP (*trans*-null) JAM-A by amide linkages and assessed for bond frequency (B), force required for rupture of homodimerizing ectodomains at different retraction speeds (C), and bond off rates by application of Bell's model (D); >500 force curves/condition, $n > 3$, ***$p < 0.001$, **$p < 0.01$, *$p < 0.05$.

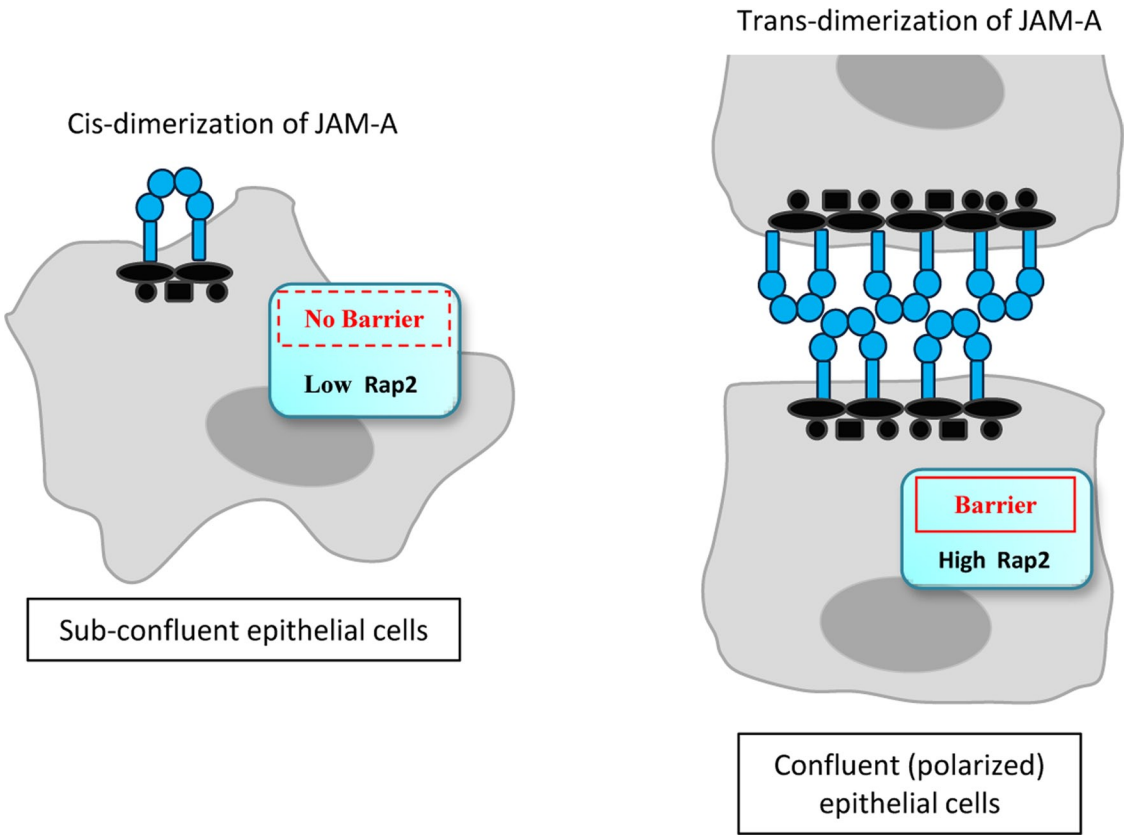

FIGURE 8: JAM-A dimerization in *cis* may initiate different signaling modalities than that initiated by JAM-A multimerization, which is dependent on *trans*-dimerization. Left, subconfluent epithelial cells may engage JAM-A *cis*-homodimers. In the absence of cell–cell contacts (no barrier), the level of active Rap2 is low. Under these conditions, cell migration and spreading are regulated by JAM-A *cis*-dimerization and increased Rap1. Right, JAM-A *trans*-dimerization in confluent monolayers of polarized epithelial cells is associated with a tight barrier. Signaling events downstream of JAM-A *trans*-dimerization lead to the activation of Rap2, which contributes to barrier regulation.

6163 JAM-A, bond life is slightly longer (lowest off rate). The higher bond stability observed between *cis*-null mutants (Figure 6C) may be attributable to the fact that *cis*-null JAM-A is not previously engaged in homodimerization and, in that way, may freely reposition until the most stable *trans*-interacting conformation is established. In support of this possibility, the results from in vitro bead-clustering experiments indicate that JAM-A *cis*-dimerization–null mutants permit bead clustering as efficiently as WT JAM-A.

In addition, disruption of JAM-A homodimerization events after treatment with J10.4 Fab′ fragments (Figure 6), which bind at residues surrounding glutamine 117 (Mandell *et al.*, 2005), suggests that J10.4 antibodies indeed disrupt JAM-A *cis*-dimerization, as previously reported (Severson *et al.*, 2008), but may also disrupt *trans*-dimerization due to steric hindrance. Intriguingly, cells treated with J10.4 antibody have decreased ability to recover barrier function after calcium switch (Liu *et al.*, 2000). These observations may suggest that J10.4 treatment affects barrier not by disrupting *cis*-dimerization, but instead by sterically disrupting JAM-A *trans*-dimerization.

Moreover, assessment of Rap2 GTPase activity (Figure 7) also suggests that *trans*-dimerization occurs independently of *cis* interactions. Indeed, if *cis*-dimerization were a prerequisite for *trans*-dimerization in cells, any phenotype requiring *trans*-dimerization would also be affected by disruption of *cis*-dimerization. However, the results shown in Figure 7 indicate that Rap2 activation is reduced by overexpression of *trans*- but not *cis*-dimerization–null mutants. As such, we cannot conclude that *trans*-dimerization requires the formation of *cis*-dimers, but that both *cis*- and *trans*-dimerization of JAM-A are required for its stabilization at cell–cell contacts, as supported by the data in Figure 3.

Our laboratory recently reported that short interfering RNA (siRNA)–mediated loss of JAM-A decreased the activity of the GTPase Rap2, resulting in enhanced epithelial permeability (Monteiro *et al.* 2013). Of interest, here we show that *trans*- but not *cis*-dimerization results in enhanced Rap2 activity (Figure 7A). The finding that JAM-A *trans*-dimerization specifically affects the activity of Rap2 independently of *cis*-dimerization implies that JAM-A *cis*- or *trans*-dimerization may act as a molecular switch, as depicted in the model shown in Figure 8. Indeed, we previously reported that JAM-A dimerization in *cis* results in activation of the GTPase Rap1, which regulates β1 integrin protein levels and cell migration (Severson *et al.* 2008, 2009). It is tempting to speculate that in populations of subconfluent cells, *cis*-dimerization of JAM-A alone does not initiate barrier-inducing signals, presumably because spreading cells lack the requisite polarized cell–cell contacts; however, they promote cell migration and spreading through preferential activation Rap1. *Trans*-dimerization of JAM-A, on the other hand, would require contact between adjacent cells, be more robust in confluent cell

populations, and facilitate recruitment of additional signaling proteins leading to the activation of Rap2. The increased Rap2 activity observed in confluent epithelial cell monolayers (Figure 7B) is consistent with *trans*-dimerization of JAM-A acting as a molecular switch to regulate epithelial barrier formation. These findings support a model in which *trans* interactions of *cis*-dimers promote assembly of a multicomponent signaling complex to regulate barrier function.

MATERIALS AND METHODS

Cell culture

CHO cells and human embryonic kidney cells (HEK-293T) were grown in DMEM supplemented to contain 10% fetal bovine serum (FBS), 2 mM L-glutamine, 100 IU of penicillin, 100 µg/ml streptomycin, 15 mM 4-(2-hydroxyethyl)-1-piperazineethanesulfonic acid, and 1% nonessential amino acids and were subcultured with 0.05% trypsin (CellGro, Manassas, VA). For reovirus infection studies, CHO cells were cultured in F12 medium supplemented to contain 10% FBS, 2 mM L-glutamine, 100 U/ml penicillin, 100 µg/ml streptomycin, and 25 ng/ml amphotericin B. Cells were transfected with 1–3 µg of plasmid DNA containing WT or mutant JAM-A constructs/10^6 cells using Lipofectamine (Invitrogen, Grand Island, NY) according to the manufacturer's instructions. Transfected cells were cultured for 48 h before assessment of JAM-A expression, Rap2 activity, immunofluorescence, or infection with reovirus.

Antibodies

The murine monoclonal anti–JAM-A antibodies 1H2A9, J10.4, and JF3.1 were purified as described (Liu *et al.*, 2000; Mandell *et al.*, 2004). Other antibodies were purchased as follows: polyclonal affinity-purified rabbit anti–JAM-A (Invitrogen), monoclonal mouse Rap2 and polyclonal affinity-purified rabbit ZO-2 (BD Transduction Laboratories, San Jose, CA), and polyclonal affinity-purified rabbit anti-afadin 02246, monoclonal mouse anti-tubulin, and polyclonal affinity-purified rabbit anti-actin (Sigma-Aldrich, St. Louis, MO). For immunoblots, horseradish peroxidase–conjugated secondary antibodies were used (Jackson ImmunoResearch Laboratories, West Grove, PA). For immunofluorescence studies, fluorescein isothiocyanate– and Alexa-conjugated antibodies (Invitrogen) were used.

Expression and purification of recombinant JAM-A

WT and *cis*-dimerization–null mutants 6163 and DL1 JAM-A in pCDNA 3.0 were cloned as previously described (Mandell *et al.*, 2004; Severson *et al.*, 2008). The NNP and KSV JAM-A point mutants were engineered using WT JAM-A in pCDNA 3.0 by overlap PCR. Initial amplification of WT JAM-A in pCDNA 3.0 was performed with primer pairs 5′-gctcggatccgccaccatggggacaaaggcgcaagt-3′ and 5′-atatctcgagtcacaccaggaatgacgaggtctg-3′. NNP and KSV point substitutions to alanines were introduced with amplification with primer pairs 5′-cctgaagtcagaattcctgaggctgctgctgtgaagttgtcctgtgcc-3′ and 5′-ggcacaggacaacttcacagcagcagcctcaggaattctgactcagg-3′ and 5′-tgccaactggtatcaccttcgcggccgcgacacgggaagacactggga-3′ and 5′-tcccagtgtcttcccgtgtcgcggccgcgaaggtgataccagttggca-3′, respectively. The inserts of *trans*-null mutants NNP and KSV were digested with *Bam*HI and *Xho*I restriction enzymes and ligated into pDNA3.0 vectors. For bacterial expression of glutathione *S*-transferase–tagged JAM-A, extracellular portions of WT, 6163, DL1, NNP, and KSV JAM-A were amplified with primer pairs 5′-atatggatccggcattgggcagtgttacag-3′ and 5′-atatctcgagctaattccgctccacagcttc-3′, followed by restriction enzyme digestion using *Bam*HI and *Xho*I and ligation into pGEX vectors. For bacterial expression of His-tagged JAM-A, extracellular portions of WT, 6163, DL1, NNP, and KSV JAM-A were amplified with primer pairs 5′-gtttaactttaagaaggagatatacatatgagtgttacagtgcactcttctgaa-3′ and 5′-gcagcggtcggcagcaggtatttcattagtgatggtgatggtgatggtgat-3′, followed by restriction enzyme digestion using SLIC *Nde*I and ligation into pET22b vectors. All JAM-A constructs were expressed in DE3 *Escherichia coli* by autoinduction and purified by gravity flow chromatography with nickel-nitriloacetic acid agarose (Qiagen,Valencia,CA) or glutathione agarose (Sigma-Aldrich), followed by dialysis in phosphate-buffered saline (PBS).

Size-exclusion chromatography

Gel filtration of WT and mutant JAM-A ectodomains was performed by loading 1 mg of each protein onto Sephacryl S100 or S300 columns (GE Healthcare, Pittsburgh, PA) at 4°C. The full-length WT and mutant proteins were resolved using calcium-free, pH 6.9 and 8 Tris buffers (20 mM Tris, 150 mM NaCl) at a rate of 1 ml/min. The WT and mutant proteins were also resolved using pH 5 or 5.6 citrate buffers (20 or 14 mM citric acid, 30 or 36 mM sodium citrate, 150 mM NaCl) at a rate of 1 ml/min. Blue dextran (3000 kDa), ovalbumin (45 kDa), chymotrypsinogen (25 kDa), and cytochrome *c* (12 kDa) were used as standards. The logarithmic correlation of the elution peak volumes of the standard proteins and the molecular weights were calculated using Excel (Microsoft). The apparent Stokes radius of the protein samples according to their peak elution volumes were calculated from the formula obtained.

Immunoblots

Cells were homogenized in radioimmunoprecipitation assay (RIPA) lysis buffer (20 mM Tris, 50 mM NaCl, 2 mM EDTA, 2 mM ethylene glycol tetraacetic acid, 1% sodium deoxycholate, 1% Triton X-100, and 0.1% SDS, pH 7.4) or 0.1% NP40 or 1% Brij 97 lysis buffer (10 mM Tris HCl pH 8.0, 150 mM NaCl, 1 mM $MgCl_2$, 1 mM $CaCl_2$) supplemented with protease and phosphatase inhibitor cocktails (Sigma-Aldrich). A bicinchoninic acid assay (Pierce) was used to determine lysate protein concentrations. Lysates were cleared by centrifugation and boiled in reducing SDS sample buffer. SDS–PAGE and immunoblots were performed using standard methods. Tubulin was used as a protein loading control.

Immunofluorescence microscopy

Cells were grown on eight-well chambered slides, washed in Hank's buffered saline solution (HBSS+; CellGro), fixed in 100% ethanol at –20°C for 20 min, and blocked in 5% BSA in HBSS+ for 1 h. Primary antibodies were diluted in blocking buffer and incubated with cells at 4°C overnight. Fluorescently labeled secondary antibodies were diluted in blocking buffer and incubated with cells at room temperature for 45 min. Stained cells were washed in HBSS+ and mounted in Prolong Antifade Agent (Invitrogen). A laser scanning microscope (LSM 510; Carl Zeiss,Thornwood, NY) was used to capture confocal fluorescence images. Images were processed using ImageJ and LSM software.

Rap2 activity assay

Rap2 activity assays were performed according to the manufacturer's instructions (Millipore, Billerica, MA, and Cell Biolabs, San Diego, CA). Cells were lysed at 4°C in a Tris and Triton X-100–based lysis buffer. Cell debris was removed by centrifugation, and 40 µl was saved as input to determine total Rap2 levels. Lysates containing equal amounts of protein for each sample (0.5–1.5 mg) were incubated at 4°C for 60 min with Ral-GDS agarose beads to bind active Rap2 (Knaus *et al.*, 2007). Beads were washed three times with lysis buffer, followed by boiling in SDS sample buffer. Samples were analyzed by immunoblotting with detection by Rap2 mAb (BD Laboratories).

Flow cytometry of JAM-A–conjugated beads

His-tagged Dynabeads (5 µl; Invitrogen) measuring 1 µm were incubated with 2 µg of WT, 6163, NNP, and KSV JAM-A in 500 µl of PBS at room temperature for 10 min. Conjugated beads were washed with PBS using magnetic racks before resuspension in 500 µl of PBS. JAM-A–induced bead aggregation was assessed by flow cytometry. Single beads were distinguished from doublets, triplets, and larger aggregates by size, as determined by light scatter. Both forward and side scatter were set to logarithmic scale.

To determine whether equivalent levels of JAM-A were bound to beads, conjugated beads were washed once with PBS and incubated with FACS buffer (2% FBS in PBS) containing JAM-A–specific monoclonal antibody J10.4. After incubation at 4°C for 30 min with rotation, cells were pelleted, washed twice with FACS buffer, and incubated with FACS buffer containing an Alexa Fluor–conjugated secondary antibody. For each condition, 10^5 events were examined. The percentage of single beads detected of the total events counted was determined using FlowJo software (Tree Star, Ashland, OR).

Reovirus infection of transfected CHO cells

WT and mutant forms of JAM-A were expressed in CHO cells and assessed for the capacity to bind reovirus. JAM-A expression in transfected CHO cells was assessed by removing cells from tissue culture plates using CellStripper (Mediatech, Manassas, VA), and pelleting cells at 1000 × g. The mean fluorescence intensity of each sample was determined using flow cytometry.

Reovirus infection of CHO cells transfected with WT and mutant forms of JAM-A was quantified after virus adsorption at a multiplicity of infection (MOI) of 100 plaque-forming units (PFUs)/cell at 37°C for 1 h. Cells were washed twice with PBS, and fresh medium was added to each well. After incubation at 37°C for 20–24 h, cells were harvested with 0.05% trypsin-EDTA (Invitrogen) at room temperature and quenched with medium collected from each respective sample. Cells were pelleted, washed once with PBS, and incubated with FACS buffer containing Alexa Fluor–conjugated reovirus-specific antiserum. The percentage of reovirus antigen–positive cells was determined using flow cytometry. Cell staining results were quantified using FlowJo software.

Atomic force microscopy

A Nanowizard III AFM (JPK Instruments, Berlin, Germany) mounted on an optical microscope (Axio Observer.D1; Carl Zeiss Microscopy, Jena, Germany) was applied to quantify JAM-A interactions by AFM. Recombinant JAM-A proteins were coupled to flexible Si_3N_4 AFM cantilevers (MLCT probes, spring constant 0.03 N/m; Bruker, Calle Tecate, CA) and mica sheets (SPI Supplies, West Chester, PA) via flexible polyethylene glycol spacers (acetal-PEG-NHS) as described (Spindler *et al.*, 2009; Wildling *et al.*, 2011). AFM cantilevers and mica were functionalized with amino groups by ethanolamine treatment and coupled to the *N*-hydroxysuccinimide ester group of the heterobifunctional linker. The acetal function of the linker was converted to an aldehyde group by citric acid treatment to allow reaction with the amino groups of JAM-A.

To measure JAM-A interactions, the AFM tip was lowered onto the mica surface and retracted again, and binding events were detected by continuously measuring the deflection of the cantilever as described (Spindler *et al.*, 2009). The AFM cantilever was moved in constant-force mode with speed of 1 µm/s in a *z*-range of 300 nm, 0.1-s delay time on the mica, and a retraction set point of 200 pN. At least 500 approach–retract cycles at 25 different positions on the mica were recorded for each cantilever/mica combination. Interactants were maintained in HBSS at 37°C. J10.4 was incubated at a concentration of 15 µg/ml for 30 min.

Statistics

All pooled data figures are representative of at least three independent experiments. Mean values were compared using an unpaired two-tailed Student's *t* test between two experimental groups. Error bars indicate SE of the mean. $p < 0.05$ was considered to be statistically significant.

ACKNOWLEDGMENTS

We thank Gopi Mohan, Alexander Robin, and Christopher Capaldo for significant technical contributions. This research was supported by National Institutes of Health grants DK061379, DK072564, and DK079392 to C.A.P., DK59888 and DK55679 to A.N., and DK064399 to C.A.P. and A.N.; Public Health Service Awards T32 GM007347 to C.M.L., F31 NS074596 to C.M.L.; R01 AI76983 and German Research Foundation grant KFO-274 to T.S. and T.S.D. and R37 AI38296 to T.S.D.; and the Elizabeth B. Lamb Center for Pediatric Research. Additional support was provided by the Vanderbilt-Ingram Cancer Center (CA68485), the Vanderbilt Flow Cytometry Shared Resource (DK058404), and the Vanderbilt Cell Imaging Shared Resource (DK20593).

REFERENCES

Antar AAR, Konopka JL, Campbell JA, Henry RA, Perdigoto AL, Carter BD, Pozzi A, Abel TW, Dermody TS (2009). Junctional adhesion molecule-A is required for hematogenous dissemination of reovirus. Cell Host Microbe 5, 59–71.

Azari BM, Marmur JD, Salifu MO, Cavusoglu E, Ehrlich YH, Kornecki E, Babinska A (2010). Silencing of the F11R gene reveals a role for F11R/JAM-A in the migration of inflamed vascular smooth muscle cells and in atherosclerosis. Atherosclerosis 212, 197–205.

Babinska AA, Kedees MHM, Athar HH, Ahmed TT, Batuman OO, Ehrlich YHY, Hussain MMM, Kornecki EE (2002a). F11-receptor (F11R/JAM) mediates platelet adhesion to endothelial cells: role in inflammatory thrombosis. Thromb Haemost 88, 843–850.

Babinska AA, Kedees MH, Athar H, Sobocki T, Sobocka MB, Ahmed T, Erhlich Y, Hussain MM, Kornecki E (2002b). Two regions of the human platelet F11-receptor (F11R) are critical for platelet aggregation, potentiation and adhesion. Thromb Haemost 87, 712–721.

Baumgartner W, Hinterdorfer P, Ness W, Raab A, Vestweber D, Schindler H, Drenckhahn D (2000). Cadherin interaction probed by atomic force microscopy. Proc Natl Acad Sci USA 97, 4005–4010.

Bazzoni G, Martínez-Estrada O, Orsenigo F, Cordenonsi M, Citi S, Dejana E (2000). Interaction of junctional adhesion molecule with the tight junction components ZO-1, cingulin, and occludin. J Biol Chem 275, 20520–20526.

Bell GI (1978). Models for the specific adhesion of cells to cells. Science 200, 618–627.

Brieher WM (1996). Lateral dimerization is required for the homophilic binding activity of C-cadherin. J Cell Biol 135, 487–496.

Ebnet K, Schulz C, Brickwedde MZ, Pendl GG, Vestweber D (2000). Junctional adhesion molecule interacts with the PDZ domain-containing proteins AF-6 and ZO-1. J Biol Chem 275, 27979–27988.

Ebnet K, Suzuki A, Horikoshi Y, Hirose T, Brickwedde M-KMZ, Ohno S, Vestweber D (2001). The cell polarity protein ASIP/PAR-3 directly associates with junctional adhesion molecule (JAM). EMBO J 20, 3738–3748.

Forrest JC (2003). Structure-function analysis of reovirus binding to junctional adhesion molecule 1: implications for the mechanism of reovirus attachment. J Biol Chem 278, 48434–48444.

Guglielmi KM, Kirchner E, Holm GH, Stehle T, Dermody TS (2007). Reovirus binding determinants in junctional adhesion molecule-A. J Biol Chem 282, 17930–17940.

Iden S, Misselwitz S, Peddibhotla SSD, Tuncay H, Rehder D, Gerke V, Robenek H, Suzuki A, Ebnet K (2012). aPKC phosphorylates JAM-A at Ser285 to promote cell contact maturation and tight junction formation. J Cell Biol 196, 623–639.

Kirchner E, Guglielmi KM, Strauss HM, Dermody TS, Stehle T (2008). Structure of reovirus sigma1 in complex with its receptor junctional adhesion molecule-A. PLoS Pathog 4, e1000235.
Knaus UG, Bamberg A, Bokoch GM (2007). Rac and Rap GTPase activation assays. In: Methods in Molecular Biology, Totowa, NJ: Humana Press, 59–67.
Kostrewa D, Brockhaus M, D'Arcy A, Dale G (2001). X-ray structure of junctional adhesion molecule: structural basis for homophilic adhesion via a novel dimerization motif. EMBO J 20, 4391–4398.
Liu Y, Nusrat A, Schnell FJ, Reaves TA, Walsh S, Pochet M, Parkos CA (2000). Human junction adhesion molecule regulates tight junction resealing in epithelia. J Cell Sci 113, 2363–2374.
Mandell KJ, Babbin BA, Nusrat A, Parkos CA (2005). Junctional adhesion molecule 1 regulates epithelial cell morphology through effects on beta1 integrins and Rap1 activity. J Biol Chem 280, 11665–11674.
Mandell KJ, McCall IC, Parkos CA (2004). Involvement of the junctional adhesion molecule-1 (JAM1) homodimer interface in regulation of epithelial barrier function. J Biol Chem 279, 16254–16262.
Monteiro AC *et al.* (2013). JAM-A associates with ZO-2, Afadin and PDZ-GEF1 to activate Rap2c and regulate epithelial barrier function. Mol Biol Cell 24, 2849–2860.
Naik MU, Naik TU, Suckow AT, Duncan MK, Naik UP (2008). Attenuation of junctional adhesion molecule-A is a contributing factor for breast cancer cell invasion. Cancer Res 68, 2194–2203.
Nava P *et al.* (2011). JAM-A regulates epithelial proliferation through Akt/β-catenin signalling. EMBO Rep 12, 314–320.
Prota AE (2003). Crystal structure of human junctional adhesion molecule 1: Implications for reovirus binding. Proc Natl Acad Sci USA 100, 5366–5371.
Severson EA, Jiang L, Ivanov AI, Mandell KJ, Nusrat A, Parkos CA (2008). *cis*-Dimerization mediates function of junctional adhesion molecule A. Mol Biol Cell 19, 1862–1872.
Severson EA, Lee WY, Capaldo CT, Nusrat A, Parkos CA (2009). Junctional adhesion molecule A interacts with afadin and PDZ-GEF2 to activate Rap1A, regulate b1 integrin levels, and enhance cell migration. Mol Biol Cell 20, 1916–1925.
Spindler V, Heupel W-M, Efthymiadis A, Schmidt E, Eming R, Rankl C, Hinterdorfer P, Müller T, Drenckhahn D, Waschke J (2009). Desmocollin 3-mediated binding is crucial for keratinocyte cohesion and is impaired in pemphigus. J Biol Chem 284, 30556–30564.
Takeda H, Shimoyama Y, Nagafuchi A, Hirohashi S (1999). E-cadherin functions as a *cis*-dimer at the cell–cell adhesive interface in vivo. Nat Struct Biol 6, 310–312.
Vedula SRK, Lim TS, Kirchner E, Guglielmi KM, Dermody TS, Stehle T, Hunziker W, Lim CT (2008). A comparative molecular force spectroscopy study of homophilic JAM-A interactions and JAM-A interactions with reovirus attachment protein σ1. J Mol Recognit 21, 210–216.
Wildling L *et al.* (2011). Linking of sensor molecules with amino groups to amino-functionalized AFM tips. Bioconjug Chem 22, 1239–1248.
Zhang B, Lim TS, Vedula SRK, Li A, Lim CT, Tan VBC (2010). Investigation of the binding preference of reovirus sigma1 for junctional adhesion molecule A by classical and steered molecular dynamics. Biochemistry 49, 1776–1786.